Negative differential magnetization for Ni nanoparticles in Al

E. Fonda,[1,*] S. R. Teixeira,[2] J. Geshev,[2] D. Babonneau,[3] F. Pailloux,[3] and A. Traverse[1]

[1]*Laboratoire pour l'Utilisation du Rayonnement Electromagnétique (LURE), Boîte Postale 34, 91898 Orsay, France*
[2]*Instituto de Física–UFRGS, P.O. Box 15051, 91501-970, Porto Alegre, RS, Brazil*
[3]*Laboratoire de Métallurgie Physique, UMR6630 CNRS, Boîte Postale 30179, 86962 Futuroscope Chasseneuil, France*

Using a layer-by-layer deposition technique, Ni thin films were sandwiched between AlO_x layers in an Al matrix. By using x-ray-absorption spectroscopy, grazing incidence small-angle x-ray scattering, and high-resolution transmission electron microscopy, we showed that the Ni layers are discontinuous and that pure Ni clusters are formed with sizes in the nanometer range. Depending on the preparation conditions, different magnetic behaviours are observed. When only one discontinuous Ni layer is grown, the hysteresis loops at low temperature display a conventional shape with a reduced magnetic moment per atom due to a magnetically dead layer at the cluster surface. When three discontinuous Ni layers are grown, a negative differential magnetization is observed. This phenomenon is interpreted as due to an antiferromagnetic coupling between two populations of magnetic grains having different average diameters in the different Ni layers. The coupling is indirect through the Al spacer.

I. INTRODUCTION

In the past two decades, new magnetic behaviors have been evidenced in relationship with lowering of the material dimensionality. In thin multilayers[1] and granular systems,[2] for example, giant magnetoresistance and ferromagnetic-antiferromagnetic (FM-AF) coupling have been observed. More recently, nanoparticles have displayed peculiar properties related to their diameter of only a few nanometers. For free clusters, a magnetic moment per atom (MMA) larger than that of the bulk has been measured,[3] whereas for clusters of the same diameter embedded in matrices, a smaller MMA has been observed.[4]

Very recently, negative differential magnetization reported in Fe layers deposited on W steps[5] and inverted hysteresis loops observed in a nanocrystalline/amorphous $Fe_{81}Nb_7B_{12}$ alloy[6] have been interpreted according to two-phase models and AF exchange interaction.

In a previous work,[7] we systematically investigated the possibility to prepare magnetic Ni clusters with a controlled average size in a nonmagnetic Al matrix. The preparation technique we used is based on the work of Egelhoff *et al.*,[8] who showed, by x-ray reflectometry, that post-oxidation suppresses intermixing at the Al/Ni interface. By x-ray-absorption spectroscopy (XAS), we determined an exposure time and air pressures for which no sign of Al/Ni intermixing or of Ni oxidation could be detected.[7] The Ni thickness was as low as 0.7 nm and the air pressure was two orders of magnitude larger than that reported by Egelhoff *et al.*[8]

In the present article, several multilayers of the type Al buffer\Ni\$(Al_x\backslash Ni)_{n-1}$\Al cap, with constant Ni thickness, have been studied. The preparation conditions have been chosen to determine the role of parameters such as air pressure, Al spacer thickness x, and number of Ni layers n, on the magnetic properties of the system. Complementary to XAS experiments, several characterization techniques have been carried out, namely high-resolution transmission electron mi-

croscopy (HRTEM), grazing incidence small-angle x-ray scattering (GISAXS), and magnetometry.

Depending on the preparation conditions, different magnetic behaviors are observed. For one Ni layer, normal hysteresis loops are measured at low temperatures indicating FM behavior and evolution towards superparamagnetism at higher temperatures as expected for small metallic clusters. For three Ni layers, a negative differential magnetization is seen in the hysteresis loops. The thicker the Al spacer, the higher the magnetic field value at which this phenomenon occurs. The possible origin of these features is discussed in terms of AF coupling between magnetic grains of different sizes belonging to the different Ni layers.

II. EXPERIMENT

We summarize the preparation conditions described in Ref. 7. The samples were deposited at LURE by electron gun evaporation either on previously cleaned Si or SiO_2 substrates. The base pressure in the chamber was 10^{-8} mbar, whereas the maximum pressure during evaporation of the Al and Ni metals was in the low 10^{-7} mbar range. After deposition of each layer, the pressure was raised in the chamber with a flux of air (20% O_2, 80% N_2, no water). The air pressure, p_{air}, was kept for 300 s, either at a value of 1×10^{-3} mbar or at 3×10^{-3} mbar. Then it was immediately lowered back to the base value. The layer thickness and deposition rate were measured by a calibrated quartz microbalance. All samples were sandwiched between an Al buffer about 52 nm thick and an Al cap about 24 nm thick. Two Al spacer thicknesses, x, were chosen, whereas the number of Ni layers was either one or three. The Ni thickness was always 1.5 nm. The quantity of deposited Al and Ni atoms was measured by Rutherford backscattering spectrometry (RBS) using 1.2 MeV He^+ ions. Preparation conditions for the samples and film thickness deduced by RBS assuming bulk density are reported in Table I together with the

TABLE I. Preparation conditions and characteristics of the samples: t_1 is the Al buffer thickness, t_2 the Al cap thickness, m and x the Al spacer number and thickness, p the air pressure (the oxidation time is always 300 s), n the number of Ni films, and e the Ni film thickness measured by RBS. We have assumed Ni bulk density and that the three Ni layers are equally thick. The deposition rates were 10^{-2} and 10^{-1} nm s^{-1} for Ni and Al layers. Last column: techniques with which the samples were characterized.

Sample label	t_1 (nm)	t_2 (nm)	m	x (nm)	p (mbar)	n	e (nm)	Techniques
Ni_{15}	2.0	2.0	/		3×10^{-3}	1	1.70	HRTEM
$(Ni_{15}Al_0)_1$	52.0	24.1	/		3×10^{-3}	1	1.70	HRTEM, XAS, GISAXS
$(Ni_{15}Al_{46})_3$	51.5	22.2	2	4.6	3×10^{-3}	3	1.45	XAS
$(Ni_{15}Al_{83})_3$	52.0	23.3	2	8.3	1×10^{-3}	3	1.60	XAS

sample label, $(Ni_{15}Al_x)_n$. One sample was specifically prepared for in-plane HRTEM characterization with one 1.5-nm-thick Ni layer, an Al buffer, and an Al cap, each 2 nm thick, deposited on a single-crystalline NaCl, called Ni_{15}.

To characterize the film morphology, HRTEM observations were done at Laboratoire de Métallurgie Physique with a JEOL 3010 high-resolution transmission electron microscope operated at 300 kV. GISAXS experiments were performed on beam line DW31B-LURE at 7.086 keV. To characterize the Ni atomic surroundings, x-ray-absorption coefficients at the Ni K edge were recorded on beam line D42-LURE with a Si(111) channel-cut monochromator in the conversion electron yield (CEY) mode at liquid nitrogen temperature.[9] Magnetization cycles at different temperatures and zero-field-cooled/field-cooled (ZFC/FC) magnetization curves were measured with a superconducting quantum interference device (SQUID) at Instituto de Física–UFRGS.

III. RESULTS

A. Structural and morphological results: XAS, HRTEM, and GISAXS

The oscillations extracted from the x-ray-absorption coefficients are compared to those of pure Ni and a thick NiO layer in Fig. 1. The oscillations measured on a sample made
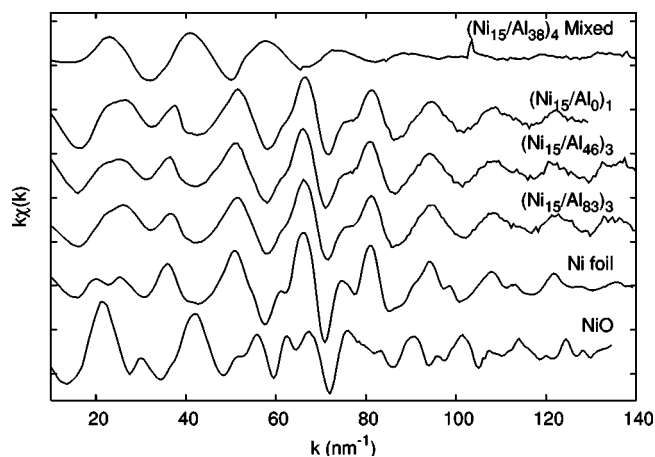

FIG. 1. EXAFS oscillations extracted from x-ray-absorption coefficients for pure Ni, NiO, a $(Ni_{15}Al_{38})_4$ spontaneously mixed system, and for the $(Ni_{15}Al_0)_1, (Ni_{15}Al_{46})_3, (Ni_{15}Al_{83})_3$ samples.

of four stacks of 1.5 nm Ni/3.8 nm Al, where Ni and Al are spontaneously mixed, are also plotted. The similarity between the oscillations for pure Ni and for the samples proves that Ni atoms in the films are mainly surrounded by other Ni atoms, rather than by Al or O atoms. The type, number of neighbors around a Ni atom, N, Ni-neighbor distances, d, and Debye-Waller factors that are indicative of atomic disorder, deduced by fitting the oscillations, are presented in Table II. As indicated by the uncertainties on N in the Table I, the number of Ni neighbors in the first shell around Ni absorbers is significantly smaller than the number of neighbors in bulk Ni (12). Ni absorbers in 1.5-nm-thick continuous layers should have 10.2 Ni neighbors for the case of perfect plane-by-plane deposition. A number of 8.9 ± 0.6 neighbors suggests discontinuous Ni layers with formation of clusters. Only in the case of the $(Ni_{15}Al_{83})_3$ sample was a small number of Al neighbors detected around the Ni atoms. No O neighbor contribution had to be introduced. When looking at the features in the Ni K edge in the x-ray-absorption coefficients, previously reported,[7] the absence of energy shift and of peaks corresponding to O neighbors confirmed the pure metallic character of the Ni clusters.

HRTEM pictures have been taken on samples with one Ni layer. The cross section taken on $(Ni_{15}Al_0)_1$ [Fig. 2(a)] shows large Al grains below and on top of the Ni discontinuous film formed of roughly spherical clusters sandwiched between AlO_x layers. One may notice that the Ni film displays some roughness induced by the first deposited Al layer. The plane-view micrograph of Ni_{15} [Fig. 2(b)] has been processed by fast Fourier transform [inset of Fig. 2(b)]. In order to distin-

TABLE II. Results of EXAFS analysis: type and number, N, of Ni nearest neighbors, d, Ni-nearest-neighbor distance, Debye-Waller factors, and D_{XAS}, average cluster diameter as obtained by the formula given in Ref. 10. All uncertainties are given in parentheses.

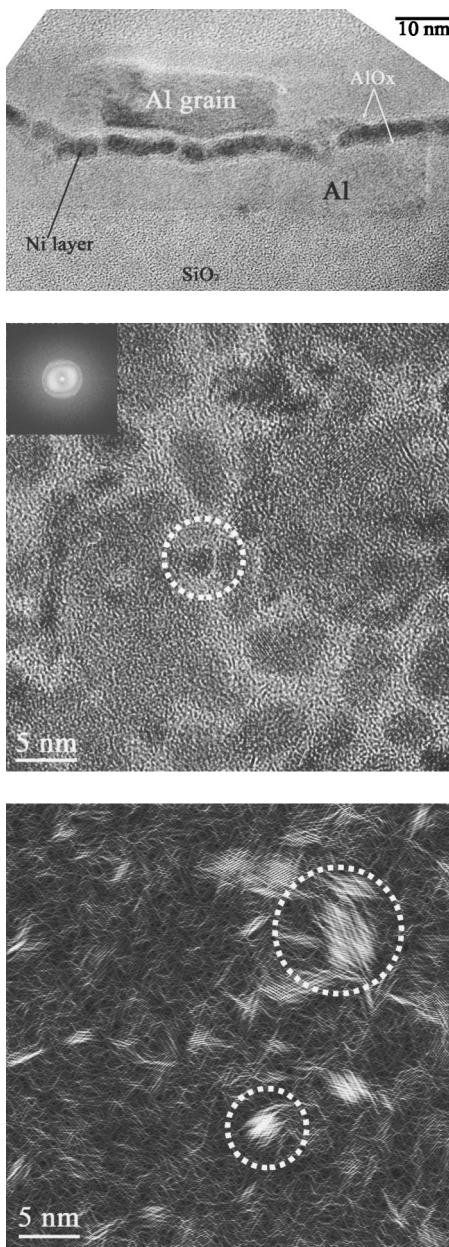| Sample label	Neighbor type	N	d (nm)	Debye-Waller factor (10^{-3} nm^{-1})	D_{XAS} (nm)
$(Ni_{15}Al_0)_1$	Ni	8.9(6)	0.2478(3)	7.3(2)	1.5(3)
$(Ni_{15}Al_{46})_3$	Ni	7.9(8)	0.2483(6)	6.6(3)	1.1(3)
$(Ni_{15}Al_{83})_3$	Al	1.1(3)	0.2420(1)	8.4(1)	
	Ni	8.7(4)	0.2479(2)	7.4(2)	1.4(4)

FIG. 3. GISAXS on $(Ni_{15}Al_0)_1$.

FIG. 2. (a) Cross-section HRTEM on $(Ni_{15}Al_0)_1$, (b) plane-view HRTEM on Ni_{15} and fast Fourier transform in the inset, and (c) Ni contribution extracted from the filtered fast Fourier transform shown in the inset of (b). One isolated Ni grain and a large particle are identified by dashed rings.

guish the Ni contribution from that due to Al, a spatial filter was applied on the ring corresponding to the Ni(111) distances. The amplitude of the inverse Fourier transform [Fig. 2(c)] shows the Ni grains. Small Ni clusters, with a spherical shape and diameter of about 2–3 nm, are isolated; others are gathered into large particles. One isolated Ni grain and a large particle are identified by dashed rings on Figs. 2(b) and 2(c).

GISAXS measurements were carried out on the $(Ni_{15}Al_0)_1$ sample. On both sides of the bright region observed in the center of the 2D pattern (Fig. 3) that is due to the sample roughness, two small diffuse lobes are detected.
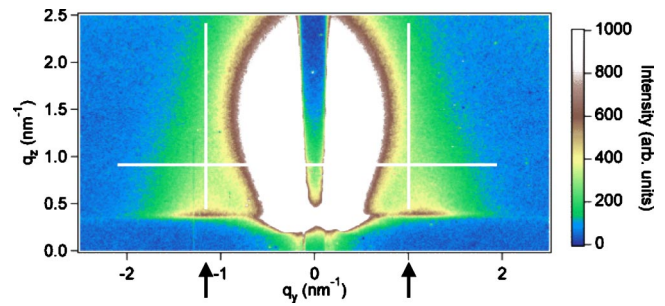
These lobes are signatures of grains in the Ni layer interacting spatially in the horizontal plane. Their location on the q_y axis provides an average distance between them of $L = 5.6$ nm. The analysis of the intensity recorded along the lines plotted parallel to the q_z and q_y axes gives an average size of $D = 3$ nm in the horizontal plane and of $H = 1.5$ nm in the vertical direction. The equivalent Ni thickness estimated from these results $e = (\pi D^2 H)/(6L^2) = 0.23$ nm is seven times smaller than the one obtained by RBS. This result suggests that smaller Ni grains are present but not detected by GISAXS. Assuming a spherical morphology, the average cluster diameter can be calculated from the number of Ni neighbors deduced by XAS.[10] All samples have similar diameters, D_{XAS}, as reported in Table II, whatever the number of Ni layers in the sample, one or three. The difference observed between the D_{XAS} values and those given by HRTEM and GISAXS will be discussed later.

B. Magnetization results: Zero-field-cooled/field-cooled curves

The ZFC-FC curves recorded on the samples for an applied magnetic field, H, of 20 Oe are compared in Fig. 4. Rather similar behaviors are seen when one compares $(Ni_{15}Al_{83})_3$ with $(Ni_{15}Al_{46})_3$ whereas the curves for $(Ni_{15}Al_0)_1$ look different. The temperature where the magnetization drops to zero, called the paramagnetic Curie temperature, T_c, is very dependent on the sample. It is always lower than the Curie temperature of pure bulk Ni (627.4 K) due to the small size of the clusters.[11] For $(Ni_{15}Al_0)_1$, T_C is around 290 K, whereas for $(Ni_{15}Al_{83})_3$ and $(Ni_{15}Al_{46})_3$ it is about 210 K (Table III).

For $(Ni_{15}Al_{83})_3$ and $(Ni_{15}Al_{46})_3$, there is a splitting between the FC-ZFC curves, typical for small clusters, occurring at a low temperature called the blocking temperature, T_b. However, above T_b, instead of a monotonic T dependence usually fitted with a Curie-Weiss law, a bump is present in both the ZFC and FC thermomagnetic curves. This bump is located at different temperatures, T', depending on the sample. Values of T_b and T' are collected in Table III. For $(Ni_{15}Al_0)_1$, T_b is higher than that for the other samples. Its ZFC thermomagnetic curve displays a bump; its T' is smaller than T_b (Table III). The existence of T_b and T' might be due to two populations of magnetic grains.

C. Magnetization results: Magnetization cycles

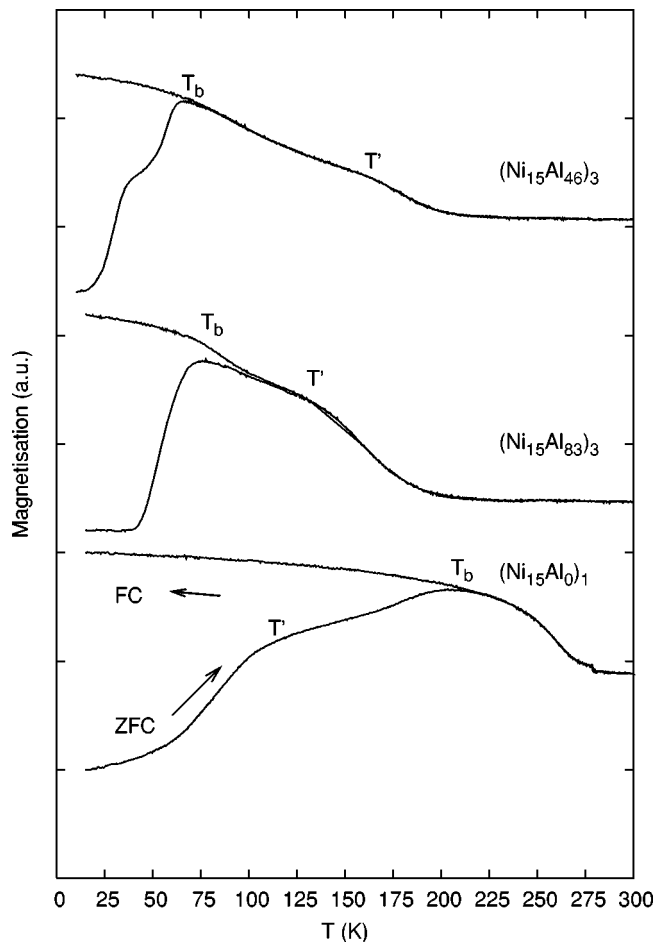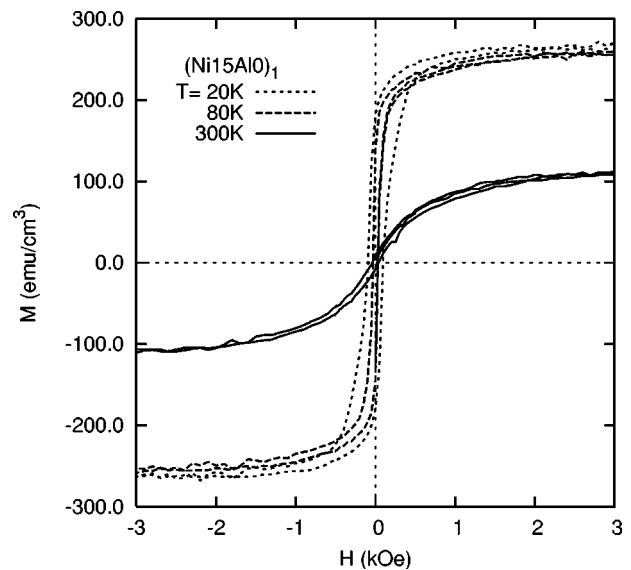The in-plane magnetization cycles for the $(Ni_{15}Al_0)_1$ sample are shown in Fig. 5 for $T=20$, 80, and 300 K. A

FIG. 4. FC-ZFC curves for the three samples.

FIG. 5. Hysteresis loops for $(Ni_{15}Al_0)_1$ at different temperatures.

ferromagnetic cycle is observed for all T with a reduction of the coercive field, H_c, when T increases. Magnetic data extracted from these curves, i.e., H_c, the remanent magnetization M_r, and the magnetization at saturation M_s, measured at $T=20$ K, are given in Table III. Note that the ratio M_r/M_s =0.74 is far above 0.64 or 0.50, which are the expected values for the noninteracting case for two- or three-dimensional random easy axis orientations, respectively, if one calculates the weighted average of the magnetization projections along the field direction.

From the saturated magnetization at low T, the MMA is calculated using the number of Ni atoms given by RBS: $0.31 \mu_B$/at, i.e., half the bulk value (Table III). A fit of the hysteresis loop at 300 K was made considering two contributions, the first coming from noninteracting superparamagnetic particles, $M^{SPM}(H)$, and the second coming from blocked large ferromagnetic grains, $M^{FM}(H)$. This latter phase was assumed as being in a saturated state with $M^{FM}_{sat}=M_r/0.866$, the value for a disordered system of Ni spherical particles.[12] The first contribution to the total magnetization should be described by a weighted superposition of Langevin functions, i.e., $M^{SPM}(H)=(M_s/V)L(\alpha)$, where $L(\alpha)=\coth(\alpha)-1/\alpha$. Here $\alpha=\mu H/k_B T$, with μ the magnetic moment of a single-domain Ni particle with saturation magnetization M_s and volume V, k_B being the Boltzmann constant. The fit provides an average diameter of the superparamagnetic particles of 30 nm with a standard deviation σ =0.30 nm (Table III).

Figure 6 shows in-plane hysteresis loops measured for the $(Ni_{15}Al_{83})_3$ sample at different temperatures (5, 80, and 250 K). A ferromagnetic hysteresis cycle is seen for $T=5$ K, is

TABLE III. Magnetic measurements results: Curie temperature, T_c, and blocking temperatures, T_b, T', deduced from the thermomagnetic curves. Coercive field, H_c, remanent magnetization, M_r, magnetization at saturation, M_{sat}, and MMA deduced from the magnetization cycles. The temperature at which the magnetization cycle was measured is 20 K for $(Ni_{15}Al_0)_1$, 10 K for $(Ni_{15}Al_{46})_3$, and 5 K for $(Ni_{15}Al_{83})_3$. Average diameter, D_{mag}, and size distribution, σ, deduced from the Langevin fits. Literature values of T_c and MMA at 5 K for bulk Ni are also given for comparison.

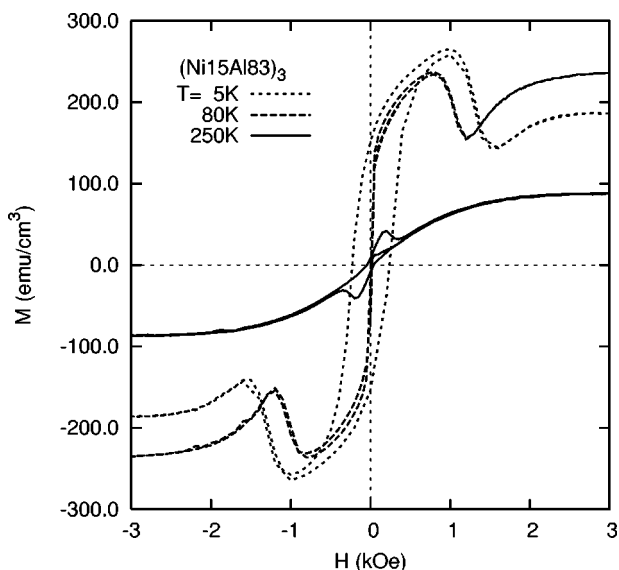| Sample label	T_c(K)	T_b(K)	T'(K)	H_c(Oe)	M_r(emu/cm^3)	M_{sat}(emu/cm^3)	MMA μ_B/at.	D_{mag} (nm)	σ (nm)
$(Ni_{15}Al_0)_1$	290	215	125	93	181	242	0.31	30	0.30
$(Ni_{15}Al_{46})_3$	220	65	163	142	193	225			
$(Ni_{15}Al_{83})_3$	210	76	134	232	151	256	0.32	26	0.15
Ni bulk	627.4						0.64		

FIG. 6. Hysteresis loops for $(Ni_{15}Al_{83})_3$ at different temperatures.

still faintly present for $T=80$ K, but disappears for higher T values. The coercive field measured at 5 K, given in Table III, is much larger than for $(Ni_{15}Al_0)_1$, and the ratio M_r/M_{sat} is equal to 0.59, much closer to 0.5. All magnetization curves demonstrate very unusual local minima and maxima in the first and third quadrants for both increasing and decreasing fields, except for the curve at 250 K where the singularity appears for the low field range in the descending branches only (Fig. 6).

A fit on the ascending branch of the magnetization cycle recorded at 250 K, with a weighted superposition of Langevin functions, provides an average magnetic diameter of 26 nm with a standard deviation $\sigma=0.15$ nm (Table III).

Figure 7 shows the first quadrant of the hysteresis loops measured for the three samples at low T. Once again, an unusual behavior is observed for $(Ni_{15}Al_{46})_3$, similar to the observation for the $(Ni_{15}Al_{83})_3$ sample, except that the minimum is located at a field value of about 400 Oe instead of 1300 Oe. Note that M reaches a maximum value that is simi-

lar for all the samples. The measured coercive field for $(Ni_{15}Al_{46})_3$ is between the values obtained for the other samples. None of the hysteresis loops exhibits field shift due to an exchange bias phenomenon attributable to a NiO shell magnetically coupled to the Ni cluster core. This result is in agreement with XAS results that indicated the absence of O neighbors around Ni atoms.[13]

IV. DISCUSSION

A. Sample structural state and morphology

Under the preparation conditions used here, the Ni layers were found to be discontinuous with Ni cluster formation. Within the precision of our XAS analysis, the Ni clusters are free from any O contamination. This conclusion is in agreement with results of Schad *et al.*,[14] who concluded that O atoms are trapped by A1.

For samples containing one Ni layer, the average sizes of the Ni clusters deduced from XAS, GISAXS, and HRTEM are approximately the same, i.e., from 1.5 to 3 nm. The differences in size are due to the varying detection sensitivity of each technique that detects different objects.[15] Large grains dominate the GISAXS pattern, whereas XAS is very sensitive to the smallest grains. HRTEM also indicates that some small clusters are isolated and others are close one to another. Furthermore, GISAXS detects that these gathered clusters are separated by average distances of about 5.6 nm, whereas the small isolated clusters are randomly distributed in the horizontal plane. Combining XAS, GISAXS, and HR-TEM, a crude picture of the arrangement of the clusters within one Ni layer is proposed in Fig. 8, where the surface not covered by Ni particles is exaggerated for the sake of clarity. Small clusters are represented, some of them randomly distributed, others are close and located at an average distance of 5.6 nm. In the zones where Ni clusters are very close, they can interact magnetically (by dipolar interaction) in accordance with the measured M_r/M_S ratio. Thus, the magnetic size is larger than the geometrical size. Indeed, the fit with the Langevin function gives a magnetic diameter about 10 times that given by XAS, GISAXS, or HRTEM. The fit with the Langevin function provides sizes and diam-
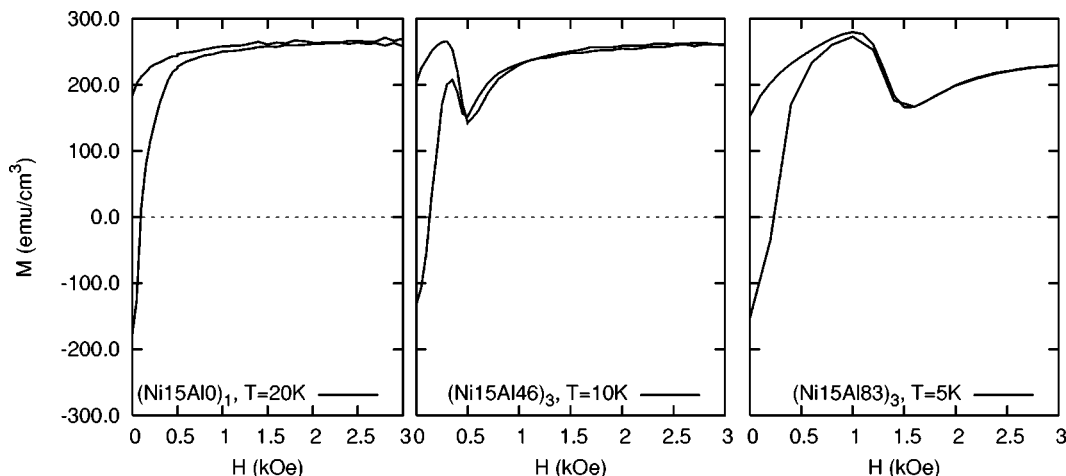

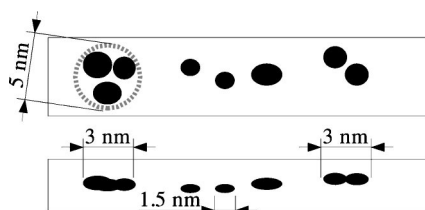FIG. 7. Comparison of hysteresis loops recorded at low temperature for the three samples.

FIG. 8. Crude picture of the clusters in one Ni layer (a) top view and (b) cross section.

eter distributions of superparamagnetic particles resulting from the dipolar interaction between smaller grains. It should be noted that the average diameters for the three samples given by XAS are similar and that the magnetic sizes for $(Ni_{15}Al_0)_1$ and $(Ni_{15}Al_{83})_3$ in the superparamagnetic regime are also similar (Table III). Hence we will assume that the crude picture of the Ni cluster arrangement proposed for one Ni layer (two types of magnetic grains: small isolated clusters and large particles resulting from close interacting clusters) is also valid for the samples containing three Ni layers.

B. Magnetic behavior

The thermomagnetic curves indicate that the samples are made of two populations of magnetic grains with different sizes, in agreement with the crude representation of Fig. 8. It is tempting from the T_b and T' values to deduce the volume values, V, through the relation $KV=25k_BT_b$, where K is the anisotropy constant. Yet it has been demonstrated[16,17] that T_b is strongly dependent on the interparticle distance. In addition, the anisotropy constant of small clusters could be very different from the bulk value.[15]

We now compare the magnetic behavior of samples made of similar clusters and particles. Two samples were made of three Ni layers in one case and a single Ni layer in the other case. Our XAS analysis showed that Ni is surrounded only by Ni atoms in samples $(Ni_{15}Al_0)_1$ and $(Ni_{15}Al_{46})_3$, whereas Ni is surrounded by Ni and some Al atoms in sample $(Ni_{15}Al_{83})_3$. This difference is likely to be related to the value of p_{air} during the postoxidation treatment (Table I). The role of p_{air} on the magnetic behavior of sample $(Ni_{15}Al_{83})_3$ was considered in our previous study.[7] Yet the new data reported here led us to consider other parameters as discussed in the following.

The MMA for the samples at low temperature (Table III) is smaller than that of bulk Ni. A similar result has been observed in other clusters, whatever the material, Ni or Co, and for different matrices such as AlN, ZrN, and Ag,[4,7,15] and was interpreted as being due to a magnetic dead layer of thickness t at the cluster surface. This thickness can be calculated from the diameter, D, given by XAS, the measured MMA, and the MMA for bulk, MMA_{bulk}, through the formula[15]

$$t=(D/2)[1-(MMA/MMA_{bulk})^{1/3}].$$

Here one finds $t=0.14$ nm in agreement with the estimates of Ref. 15 between 0.1 and 0.2 nm. It was shown that a layer of Al_2O_3 is terminated by Al atoms and not by O ones.[18] This

result agrees with what is observed in sample $(Ni_{15}Al_{83})_3$. Hence, the Ni atoms located at the cluster surface can experience a hybridization of their d electrons with s and p electrons of Al, leading to the magnetic dead layer.

Since the samples had similar grain sizes, it is surprising to find different Curie temperatures (Table III). The influence of the interlayer exchange coupling on T_c has been studied theoretically[19] and compared to experimental data for 0.73 nm Ni layers separated by Au (Ref. 20) demonstrating that fluctuations in the spacer thickness induce a depression in T_c as compared to the value for no coupling provided that the spacer thickness, x, is larger than about 1 nm. For smaller spacer thickness, both calculations[19] and experiments[20] show an increase of T_c. Although the order of magnitude of the T_c modification is larger in our case, it could be an indication of interlayer coupling in samples $(Ni_{15}Al_{83})_3$ and $(Ni_{15}Al_{46})_3$.

Similar local peaks to those observed for $(Ni_{15}Al_{83})_3$ and $(Ni_{15}Al_{46})_3$ have also been seen in the descending hysteresis loop branches in iron films deposited on Si(111) and on W(100), where the singularities have been explained in terms of vicinal surfaces and competing anisotropies in a continuous film[21] and intralayer AF coupling between nanodomains,[5] respectively. Such considerations, however, may not be readily applied to our samples since, at temperatures higher than approximately 80 K, their magnetic behavior is superparamagnetic and not ferromagnetic, as in the works quoted above. Our interpretation of the observed peculiar magnetization curves is presented below. Note that before experiencing this decrease, the cycles reached a saturation value comparable to that for the $(Ni_{15}Al_0)_1$ sample (Fig. 7).

Let us, as an example, consider the first quadrant of the magnetization cycle measured at 80 K for sample $(Ni_{15}Al_{83})_3$, plotted in the top panel of Fig. 9. In order to qualitatively explain the observed singularities based on the above considerations, we propose a model in which the magnetic system consists of two types of single-domain Ni grains that, under certain conditions, could be coupled antiferromagnetically. Similar models have been considered in Refs. 5,6. The two types of single-domain Ni grains are of different size, the larger, more "stable" ones of volume V_A and the smaller, more "unstable" of volume V_B with, for simplicity, $V_A=10$ V_B.

At sufficiently high temperatures, both A and B grains are superparamagnetic. Their magnetization curves, for the noninteracting case, can be described by Langevin functions. The dashed and dotted curves in Fig. 9(b) are examples of such functions. A schematic illustration of the evolution of the magnetic moment orientations as a function of H is given in the same panel, where the directions of the magnetic moments are represented by black and gray arrows for A and B grains, respectively. The number of arrows is considered to be proportional to the volume fractions of the magnetic phases. For the sake of simplicity of the figure, the evolution of the smaller grain's magnetization orientations is shown only since the mean direction of the larger ones does not change drastically with H. In the low field range, the thermal activation dominates the magnetic state of the system and its magnetization is simply the weighted average of the two
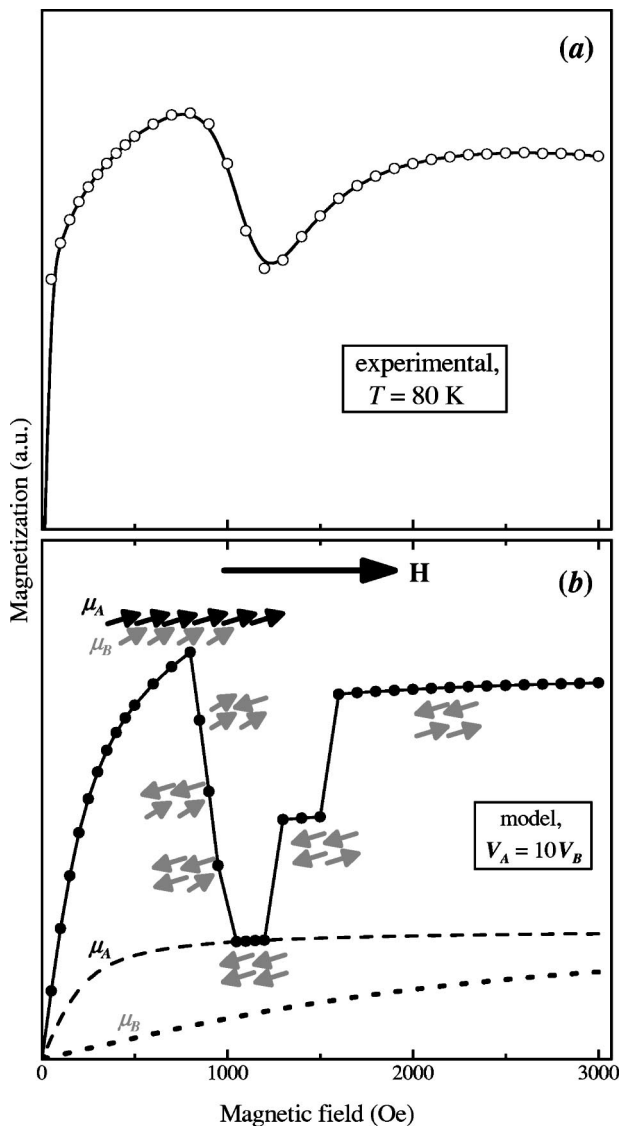
FIG. 9. Representative ($T=80$ K) magnetization curve vs external field for sample $(Ni_{15}Al_{83})_3$. (a) Experimental data (the line is a guide to the eye). (b) Schematic diagram giving the magnetic moment orientations at different points on the curve expected during their reversal as a function of H according to the model described in the text. The spin orientations are represented by black and gray arrows, corresponding to the A and B grain magnetizations, respectively. The number of arrows is proportional to the volume fraction of each magnetic phase. The dashed and dotted curves give the Langevin functions corresponding to noninteracting grains of types A and B, respectively.

Langevin functions. We now assume that fields higher than 800 Oe are sufficient to make a few of the smaller grains more stable. For some grains, the AF coupling is thus "triggered" and, assuming for simplicity that there are only A-B effectively coupled pairs, their magnetic moments are antiparallel, thus leading to a decrease of the total magnetization. This is schematically demonstrated in Fig. 9(b) by means of the switch of the gray arrows as H is raised up to ∼1000 Oe, for which all μ_B moments are orientated opposite to the adjacent μ_A moments. Further increase of the magnetic field

can yet again lead to parallel A-B moment orientations through the spin-flopping, characteristic for antiferromagnets.

Our interpretation is based on the fact that some moments could be coupled antiferromagnetically. Note that the process is initiated for different H in $(Ni_{15}Al_{83})_3$ and $(Ni_{15}Al_{46})_3$. We recall that the differences between $(Ni_{15}Al_{83})_3$ and $(Ni_{15}Al_{46})_3$ are the Al spacer thickness and the pressure during the postoxidation process, respectively, 10^{-3} mbar and 3×10^{-3} mbar. Since sample $(Ni_{15}Al_0)_1$ has also been deposited under 3×10^{-3} mbar but does not display the negative differential magnetization, this parameter is not pertinent. One notices that $(Ni_{15}Al_{83})_3$ and $(Ni_{15}Al_{46})_3$ are made of three Ni films whereas $(Ni_{15}Al_0)_1$ is made of one Ni film only. Hence it is reasonable to consider magnetic interlayer interactions as responsible for this AF coupling. An indication of such a coupling is given by the T_c evolution as discussed above. In addition, the thinner the spacer, the smaller the applied magnetic field for which the coupling takes place. In stacks made of $Ni_{81}Fe_{19}/Al_2O_3$ layers, Stanciu et al.[22] showed that for an Al_2O_3 spacer thickness of 3.1 nm, there is no longer dipolar coupling between the metallic layers. Coupling between layers could be of a Ruderman-Kittel-Kasuya-Yosida[23] (RKKY) type, or due to a pinhole in the spacer. A calculation by Qiang et al.[24] of the RKKY interaction between two Co clusters of 141 atoms embedded in a Cu matrix displays the usual oscillatory behavior versus the distance, d, between them with a the coupling constant nearly vanishing for d about 4 nm. Because of the Al spacer thickness in our samples, these hypotheses are not likely. However, in a system of isolated Co grains of diameter 4 nm embedded in SiO_2, Sankar et al.[25] showed the existence of regions antiferromagnetically aligned that are separated by a distance of 55 nm, i.e., much larger than the Al thickness in our samples. Another possibility is to consider correlated roughness between successive interfaces, as was done in Ref. 26.

The assumption of two populations of interacting magnetic grains having different sizes is in agreement with thermomagnetic curves. It also explains the difference between the size-distribution functions (not shown here) of the samples estimated from the Langevin fittings. The mean size and σ values are smaller for the sample with three Ni layers (Table III). This can be qualitatively understood by considering that if two grains are coupled, the larger one, due to the interaction with the more unstable smaller grain, will behave as a more unstable one as well. Consequently, the A-grain size estimated from the fit of the magnetization curve will be smaller than the actual one. Similarly, a B-type grain will be sensed as a larger one by the fit, since it will be effectively more stable, as compared to the noninteracting case, thus effectively decreasing σ. Yet at this step, whether the two interacting populations are those we have called the clusters as being the B grains and the particles as being the A ones is not fully demonstrated. Since this is the interlayer interaction that is responsible for the coupling, the role of the spacer thickness, respectively, 4.6 nm and 8.3 nm, might be predominant because it fixes a specific distance between the two populations of magnetic grains, whereas within a layer the
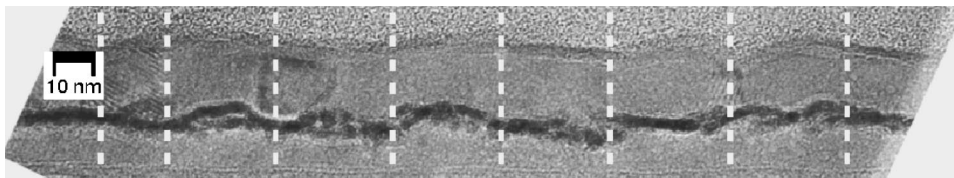
FIG. 10. Cross-section TEM on $(Ni_{15}Al_0)_1$. The aluminum grains of the thick buffer layer have a characteristic lateral size that induces a somewhat regular roughness of the film as suggested by the hand traced vertical lines. The average spacing is of about 20 nm.

grain organization is random. Note that when the interacting grains are in contact as in Ref. 27, the interaction has a FM character.

The reason for having two different magnetic size scales for the Ni grains has not been clarified, yet. The Al grains could play a role, since they induce a certain roughness. Indeed, Al grains observed on a TEM cross section (Fig. 10) have a quite regular lateral size of about 20 nm. This size compares well with the size of the larger magnetic domains. In this case, we can imagine that besides a large number of "isolated" particles, there are more dense ferrocoupled domains on the flat top of the Al grains.

V. CONCLUSION

We have studied the structural and magnetic properties of small Ni clusters prepared by a layer-by-layer deposition technique. Thanks to a post-oxidation treatment after each layer deposition,[7,8,14] and because the Ni layers are thin enough, clusters are formed sandwiched between AlO_x in an Al matrix.

The main goal of this paper was to present the very unusual local minima and maxima in the first and third quadrants of the magnetization curves for both increasing and decreasing applied magnetic fields. These minima and maxima have been observed in the three-layer systems and not in the sample with one Ni layer. This phenomenon is interpreted as due to an AF coupling between two populations of Ni grains, belonging to different Ni layers separated by specific Al thickness and having different sizes and hence different behaviors when submitted to the applied magnetic field. The proposed model leads to a magnetization curve in good qualitative agreement with the experimental one, despite the simplifications.

To reach a better understanding of the coupling between the Ni layers, the role played by several parameters has to be investigated. The roughness, especially if it is correlated from one layer to the other, could be of importance.[26] Among the other parameters, one may quote the nature and thickness of the magnetic material as well as of the spacer.

ACKNOWLEDGMENTS

*Present address: Synchrotron-Soleil, L'Orme des Merisiers, Saint-Aubin-BP48, 91192 Gif sur Yvette Cedex, France.

[1] M. N. Baibich, J. M. Broto, A. Fert, F. Nguyen van Dau, F. Petroff, P. Etienne, G. Creuzet, A. Friederich, and J. Chazelas, Phys. Rev. Lett. **61**, 2472 (1988); G. Binash, P. Grünberg, F. Saurenbach, and W. Zinn, Phys. Rev. B **39**, 4828 (1989).

[2] A. E. Berkowitz, J. R. Mitchell, M. J. Carey, A. P. Young, S. Zhang, F. E. Spada, F. T. Parker, A. Hütten, and G. Thomas, Phys. Rev. Lett. **68**, 3745 (1992); J. Q. Xiao, J. S. Jiang, and C. L. Chien, *ibid.* **68**, 3749 (1992); B. Dieny, A. Chamberod, J. B. Genin, B. Rodmacq, S. R. Teixeira, S. Auffret, P. Gerard, O. Redon, J. Pierre, R. Ferrer, and B. Barbara, J. Magn. Magn. Mater. **126**, 433 (1993).

[3] J. P. Bucher, D. C. Douglass, and L. A. Bloomfield, Phys. Rev. Lett. **66**, 3052 (1991); I. M. L. Billas, A. Châtelain, and W. A. de Heer, Science **265**, 1682 (1994); S. E. Apsel, J. W. Emmert, J. Deng, and L. A. Bloomfield, Phys. Rev. Lett. **76**, 1441 (1996).

[4] D. A. Eastham, Y. Qiang, T. H. Maddock, J. Kraft, J-P Schille, G. S. Thompson, and H. Haberland, J. Phys.: Condens. Matter **9**,
L497 (1997); D. Zanghi, C. M. Teodorescu, F. Petroff, H. Fischer, C. Bellouard, C. Clerc, C. Pélissier, and A. Traverse, J. Appl. Phys. **90**, 6367 (2001); M. Jamet, V. Dupuis, P. Mélinon, G. Guiraud, A. Perez, W. Werndorfer, A. Traverse, and B. Baguenard, Phys. Rev. B **62**, 493 (2000).

[5] Y. Yao, H. C. Mireles, J. Liu, Q. Niu, and J. L. Erskine, Phys. Rev. B **67**, 174409 (2003).

[6] E. E. Shalyguina, I. Skorvanek, P. Svec, V. A. Mel'nikov, and N. M. Abrosimova, J. Exp. Theor. Phys. **99**, 544 (2004).

[7] E. Fonda, D. Babonneau, F. Pailloux, S. R. Teixeira, and A. Traverse, Phys. Scr., T **115**, 837 (2005).

[8] W. F. Egelhoff, Jr., P. J. Chen, R. D. McMichael, C. J. Powell, R. D. Deslattes, F. G. Serpa, and R. D. Gomez, J. Appl. Phys. **89**, 5209 (2001).

[9] J. Mimault, J. J. Faix, T. Girardeau, M. Jaouen, and G. Tourillon, Meas. Sci. Technol. **5**, 482 (1994).

[10] M. Borowski, J. Phys. IV **7**, C2-259 (1997).

[11] C. M. Schneider, P. Bressler, P. Schuster, J. Kirschner, J. J. de Miguel, and R. Miranda, Phys. Rev. Lett. **64**, 1059 (1990).

[12] R. Gans, Ann. Phys. **15**, 28 (1932).

[13] M. Gruyters, J. Magn. Magn. Mater. **248**, 248 (2002).

[14] R. Schad, K. Mayen, J. McCord, D. Allen, D. Yang, M. Tondra, and D. Wang, J. Appl. Phys. **89**, 6659 (2001).

[15] A. Traverse and S. R. Teixeira, Recent Res. Dev. Magn. Magn. Mater. **1**, 521 (2003).

[16] R. W. Chantrell, N. Walmsley, J. Gore, and M. Maylin, Phys. Rev. B **63**, 024410 (2000).

[17] D. Kechrakos and K. N. Trohidou, Appl. Phys. Lett. **81**, 4574 (2002).

[18] H.-J. Freund, Surf. Sci. **500**, 271 (2002).

[19] H. Moradi and G. A. Gehring, J. Magn. Magn. Mater. **251**, 80 (2002).

[20] G. Bayreuther, F. Bensch, and V. Kottler, J. Appl. Phys. **79**, 4509 (1996).

[21] M. Cougo dos Santos, J. Geshev, J. E. Schmidt, S. R. Teixeira, and L. G. Pereira, Phys. Rev. B **61**, 1311 (2000).

[22] V. Stanciu, J. L. Soroka, J. Lu, B. Hjorvarsson, and P. Nordblad, J. Magn. Magn. Mater. **286**, 446 (2005).

[23] M. A. Ruderman and C. Kittel, Phys. Rev. **96**, 99 (1954); T. Kasuya, Prog. Theor. Phys. **16**, 45 (1956); K. Yosida, Phys. Rev. **106**, 893 (1957).

[24] Y. Qiang, R. F. Sabiryanov, S. S. Jaswal, Y. Liu, H. Haberland, and D. J. Sellmayer, Phys. Rev. B **66**, 064404 (2002).

[25] S. Sankar, D. Dender, J. A. Borchers, David J. Smith, R. W. Erwin, S. R. Kline, and A. E. Berkowitz, J. Magn. Magn. Mater. **221**, 1 (2000).

[26] J. Moritz, F. Garcia, J. C. Toussaint, B. Dieny, and J. P. Nozières, Europhys. Lett. **65**, 123 (2004).

[27] M. Cougo dos Santos, J. Geshev, L. G. Pereira, M. C. M. Alves, J. E. Schmidt, and P. Allongue, Phys. Rev. B **70**, 104420 (2004).